JOURNAL OF SOLID STATE CHEMISTRY 38, 97–104 (1981)

Defect Structures in the Brannerite-Type Vanadates. III. Preparation and Study of $Cu^{2+}_{1-x-y}Cu^{1+}_{y}\phi_{x}V_{2-2x-y}Mo_{2x+y}O_{6}$ ($x_{max} = 0.23$; $y_{max} = 0.27$)

TADEUSZ MACHEJ, ROMAN KOZŁOWSKI, AND JACEK ZIÓŁKOWSKI*

Institute of Catalysis and Surface Chemistry, Polish Academy of Sciences, ul. Niezapominajek, 30-239 Krakow, Poland

Received May 20, 1980; in final form September 10, 1980

Phases of the formula $Cu^{2+}_{1-x-y}Cu^{1+}_{y}\phi_{x}V_{2-2x-y}Mo_{2x+y}O_{6}$, where ϕ_x represents a vacancy at Cu^{2+} site, have been synthesized and characterized by X-ray diffraction, DTA, and magnetic susceptibility measurements. The extent of their homogeneity range has been established. All crystallize in the structure closely related to the brannerite type with the symmetry reduced from monoclinic to triclinic because of a Jahn–Teller distortion of CuO_6 octahedra. On heating they undergo a phase transformation to a monoclinic phase. Unit cell dimensions and transition temperatures were compiled for eight samples of the solid solution, and correlations were established between the chemical composition (x, y) and the structural parameters. Changes in unit cell parameters involve the expansion of the lattice and the systematic evolution of the triclinic unit cell to the monoclinic one.

Introduction

Cupric metavanadate, CuV_2O_6, is known to crystallize in two modifications. The low-temperature α form is triclinic $C\bar{1}$ (unconventional setting of $P\bar{1}$), with a = 9.168(5), b = 3.543(3), c = 6.478(7) Å, α = 92.25(8), β = 110.34(7), γ = 91.88(6)° (*1*). The structure is closely related to that of a series of monoclinic MV_2O_6 compounds (M = Mg, Mn, Co, Cd, Zn, Hg) belonging to the brannerite type (*2*). In this structure, both M^{2+} and V^{5+} ions are octahedrally coordinated. VO_6 octahedra, sharing three edges, form anionic sheets parallel to the (001) plane. M^{2+} ions, binding these sheets together, are located in octahedral interlayer positions. MO_6 groups share two edges, with MO_6 groups symmetrically related by a b-axis translation, forming chains parallel to this axis.

If Cu^{2+} ions are introduced into M^{2+} sites, the MO_6 octahedra exhibit a strong Jahn–Teller distortion (Fig. 1), leading to an irregular square-plane coordination of four oxygen ligands at the distance of 1.90 and 2.05 Å, with the two additional O atoms only weakly bound at 2.44 Å. The elongated axes of the octahedra, inclined to the square plane, orient parallel to each other. This strong Jahn–Teller effect destroys the original monoclinic symmetry characteristic of the brannerite-type compounds, and leads to a triclinic, distorted unit cell.

On heating, CuV_2O_6 transforms gradually from the initial triclinic α phase into the high-temperature monoclinic β phase (*3*). The transformation may be easily followed

* To whom correspondence should be addressed.

0022-4596/81/070097-08$02.00/0

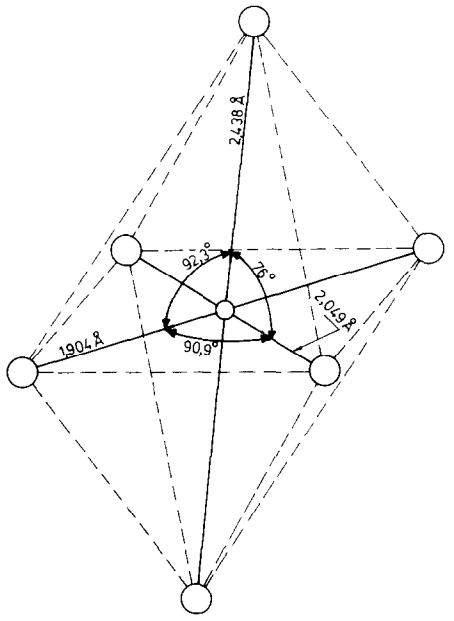

FIG. 1. Jahn–Teller distortion of CuO_6 groups in CuV_2O_6.

since in the course of temperature rise the reflections with hkl and $h\bar{k}l$ indexes, clearly separated at room temperature, shift continuously towards each other and overlap above 625°C. A DTA examination shows a weak endothermal peak at 628°C supporting additional evidence for such a transformation. At this temperature the obtained high-temperature modification may be described by a monoclinic brannerite-type unit cell with parameters $a = 9.27(1)$, $b = 3.548(4)$, $c = 6.525(6)$ Å, and $\beta = 108.8(1)°$. The described phase transition exhibits an apparent second-order character and probably involves a dynamic equilibration of the long and short bond length leading to regular CuO_6 octahedra in time average. Such transitions to a dynamic distortion are commonly encountered in oxide systems containing Jahn–Teller ions (*4*).

In recent papers (*2*, *5*) we have pointed out that one may introduce into the brannerite-type vanadates ion combinations which simultaneously give rise to cation vacancies at M sites, a type of defect to which the brannerite structure is particularly tolerant. The following solid solutions have been identified so far: $M_{1-x}\phi_x V_{1-x}Mo_{1+x}O_6$ (M = Li, Na, K, Ag) (*6*, *7*) and $Mn_{1-x}\phi_x V_{2-2x}Mo_{2x}O_6$ (*2*, *5*), in which Mo^{6+} ions replace at random V^{5+} ions. The highest concentration of the M-site vacancies ranged from 12 mole% (Li) to 45 mole% (Mn).

The aim of the present work was to prepare and characterize possible solid solutions in the CuV_2O_6–MoO_3 system. In analogy to the Mn-containing system, these solutions might be expected to be $Cu^{2+}_{1-x}\phi_x V^{5+}_{2-2x}Mo^{2+}_{2x}O_6$. However, our preliminary syntheses failed to produce single phases of this composition and we have examined the formula $Cu^{2+}_{1-y}Cu^{1+}_{y}V^{5+}_{2-y}Mo^{6+}_{y}O_6$, where charge compensation requirement is met in a different way. Finally the existence of mixed-type charge compensation solid solution of the general formula $Cu^{2+}_{1-x-y}Cu^{1+}_{y}\phi_x V_{2-2x-y}Mo_{2x+y}O_6$ was established.

Experimental

The solid solutions under study were prepared by two methods with the use of the p.a. grade, commercial reactants.

(1) The "dry" method consisted in the air heating (520–600°C, 20–60 hr with several intergrindings) of the appropriate mixtures of CuO, V_2O_5, and MoO_3. Sometimes instead of commercial CuO, a fresh "CuO" preparation was used, obtained by thermal decomposition of basic copper carbonate at 250°C for 5 hr and containing still 3.5% volatiles. The dry method, however, did not produce a single phase from the mixture of CuO/V_2O_5 = 1:1, yielding, even on prolonged heating at 520–600°C, a mixture of CuV_2O_6, $Cu_2V_2O_7$, and V_2O_5.

(2) To overcome this difficulty, the "wet" method has been developed, which

yield both homogeneous CuV_2O_6 and CuV_2O_6–MoO_6 solid solutions. NH_4VO_3, "CuO," and $(NH_4)_6Mo_7O_{24} \cdot 4H_2O$ were combined in an aqueous solution of ammonia (1:1) in such a way as to obtain a thick pulp. The pulp was dried at 80°C for 2 hr and heated up to 500°C at a rate of 10°C/min. The product was ground and annealed at 520–580°C for 40–60 hr with several intergrindings.

The DTA and X-ray examination have been carried out as described in Refs. (*2*, *5*). The phase identification was based upon the published patterns or single-crystal data for CuO, V_2O_5, MoO_3 (*8*), $CuMoO_4$ (*9*, *10*), α-CuV_2O_6 (*1*), β-CuV_2O_6 (*3*), α-$Cu_2V_2O_7$ (*11*), and β-$Cu_2V_2O_7$ (*12*).

Thermogravimetric experiments were performed with a 4102-type Sartorius thermobalance (sensitivity of 10^{-6} g) under 160 Torr pressure of oxygen, using samples of 200 mg.

Magnetic susceptibility was measured between 170–300 K using the Gouy method as described in (*13*, *14*) and tris (ethylenediamine) nickel (II) thiosulfate as calibrant ($10^6\chi_g$ = 10.82 at 25°C) (*15*). The susceptibility, which was found to be independent of the field strength, was determined at H = 4 kOe. The correction for the susceptibility of the glass tube was determined experimentally, and the diamagnetic corrections were calculated according to Klemm's method (*16*).

Results and Discussion

(i) Homogeneity Range of the Solid Solutions

Preliminary experiments aimed at establishing the chemical composition of the solid solutions in the CuV_2O_6–MoO_3 system were performed with mixtures of CuO, V_2O_5, and MoO_3 taken in the quantities corresponding to the formulas: $Cu^{2+}_{1-x}\phi_xV_{2-2x}Mo_{2x}O_6$ (x type), $Cu^{2+}_{1-y}Cu^{1+}_yV_{2-y}Mo_yO_6$ (y type), and $Cu^{2+}_{1-x-y}Cu^{1+}_y\phi_xV_{2-2x-y}Mo_{2x+y}O_6$ (xy type). In the last case $x = y$ was arbitrary chosen.

Table I summarizes the final phase composition of the studied mixtures after prolonged heating. The x-type mixtures contain an excess of V_2O_5 in relation to the true composition of solid solution formed, and the y-type mixture contain an excess of copper oxide which, apparently due to the thermodynamic preferences, appears as $CuMoO_4$ instead of CuO. As to the xy-type series, the mixture $x = 0.2$, $y = 0.2$ yields the homogeneous solid solution. The composition $x = 0.25$, $y = 0.25$ evidently lies outside the stability range of the solution in the direction of MoO_3 excess; the results obtained for the samples with lower Mo content ($x + y < 0.4$) indicate that homogeneous solid solutions are formed when $x < y$.

The above observations may be generalized in the following manner. If the initial mixture contains an excess of V_2O_5 or CuO (exactly $CuMoO_4$), the reactions obey Eqs. (1) and (2) respectively:

$$\begin{aligned}(1 - x')\mathrm{CuO} &+ (1 - x' - y'/2)\mathrm{V_2O_5} + (2x' + y')\mathrm{MoO_3} \\ &= F\ \mathrm{Cu^{2+}_{1-x-y}Cu^{1+}_y}\phi_x\mathrm{V_{2-2x-y}Mo_{2x+y}O_6} \\ &\quad + [(1 - x' - y'/2) - F(1 - x \\ &\quad - y/2)]\mathrm{V_2O_5} + F(y/4)\mathrm{O_2}, \quad (1)\end{aligned}$$

and

$$\begin{aligned}(1 - x')\mathrm{CuO} &+ (1 - x' \\ &- y'/2)\mathrm{V_2O_5} + (2x' + y')\mathrm{MoO_3} \\ &= F\ \mathrm{Cu^{2+}_{1-x-y}Cu^{1+}_y}\phi_x\mathrm{V_{2-2x-y}Mo_{2x+y}O_6} \\ &\quad + [(1 - x') - F(1 - x)]\mathrm{CuMoO_4} \\ &\quad + F(y/4)\mathrm{O_2}, \quad (2)\end{aligned}$$

where (x', y') denote the composition of the intended solid solution, (x, y) the composition of the solution really formed, and F the mole number of the latter. Equations (1)

TABLE I

PHASE COMPOSITION OF THE SOLID-STATE REACTION PRODUCTS IN THE MIXTURES OF CuO, V_2O_5, AND MoO_3[a]

A. Intended composition: $Cu_{1-x}\phi_xV_{2-2x}Mo_{2x}O_6$ (x type)

x	0.05	0.10	0.15	0.20	0.25	0.30	0.35
Phase composition	α–S, trace of V	α–S,V[b]	α–S,V	α–S,V	α–S,V	α–S,V	α–S,V,*M*

B. Intended composition: $Cu^{2+}_{1-y}Cu^{1+}_yV_{2-y}Mo_yO_6$ (y type)

y	0.10	0.20	0.30	0.40	0.50	1.0
Phase composition	α–S	α–S,*CM*[c]	α–S,*CM*	α–S,*CM*	α–S,*CM*	α–S,*CM*

C. Intended composition: $Cu^{2+}_{1-x-y}Cu^{1+}_y\phi_xV_{2-2x-y}Mo_{2x+y}O_6$ (xy type)

x	0.05	0.10	0.15	0.20	0.25
y	0.05	0.10	0.15	0.20	0.25
Phase composition	α–S trace of V	α–S trace of V	α–S trace of V	α–S	α–S,*M*

Note V–V_2O_5, *M*–MoO_3, *CM*–$CuMoO_4$, α–S solid solution of MoO_3 in α–CuV_2O_6 identified due to the shift of some X-ray reflection positions with respect to those of pure CuV_2O_6.

[a] As determined at room temperature after the following thermal treatment of the mixtures: (530°C, 20 hr) + (550°C, 20 hr) + (570°C, 20 hr).

[b] The content of V increases along the series.

[c] The content of *CM* increases along the series.

and (2) make it possible to determine the boundaries of the stability range of the xy-type solid solution from the set of simple stoichiometric relations:

balance of MoO_3	$2x' + y' = F(2x + y)$	(1a)
balance of CuO	$1 - x' = F(1 - x)$	(1b)
oxygen evolved	$F(y/4) = A$	(1c)
balance of V_2O_5	$1 - x' - y'/2 = F(1 - x - y/2)$	(2a)
balance of $CuMoO_4$	$(1 - x') - F(1 - x) = (2x' + y') - F(2x + y)$	(2b)
oxygen evolved	$F(y/4) = A$	(2c)

if only the quantity A of oxygen evolved is determined experimentally.

The gravimetric method has been used to determine the aggregate oxygen loss (A) as a function of the reaction mixture composition (x', y'). The reaction between V_2O_5, MoO_3, and "CuO" was carried out at 560°C for a period of time ensuring its completion. X-Ray analyses of the products present on termination of the heating indicated if reaction (1) or (2) took place in a given mixture. x and y factors have been calculated from x', y', and A with the aid of (1a), (1b), (1c) or (2a), (2b), (2c) sets with the accuracy of ±5%. The results obtained, presented in Fig. 2a, reveal the stability field of the xy-type solid solutions formed in CuV_2O_6–MoO_3 system. A formal "ternary

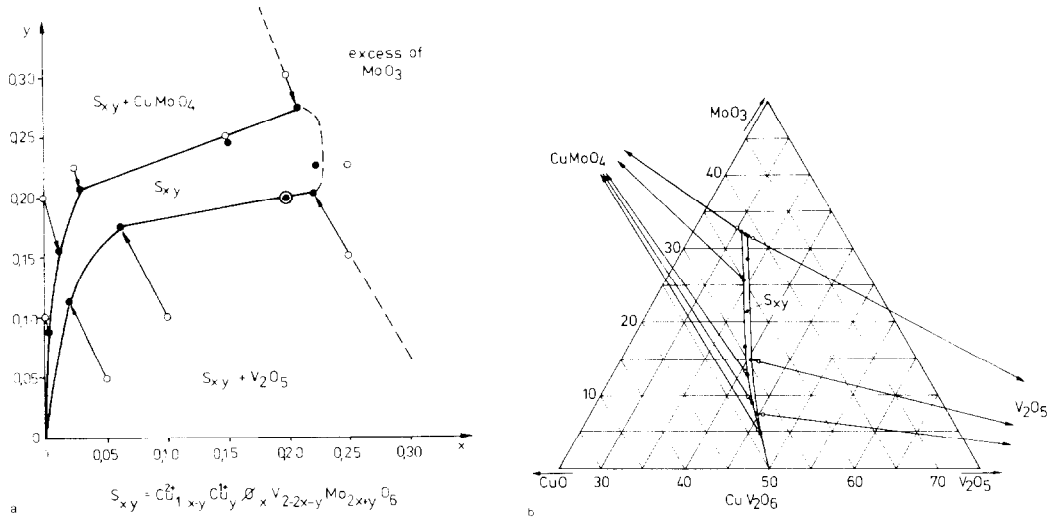

FIG. 2. (a) Stability field of $Cu^{2+}_{1-x-y}Cu^{1+}_{y}\phi_x V_{2-2x-y}Mo_{2x+y}O_6$ (S_{xy}). (b) Formal ternary phase diagram of the $CuO-V_2O_5-MoO_3$ system. Open circles represent the nominal compositions of solid solutions, black circles represent their real composition as found with the gravimetric method. The respective pairs of points are joined with arrows (tie lines).

phase diagram," in which we do not distinguish two valence states of Cu (+1 and +2), was constructed in Fig. 2b. It is easily seen that points (x', y') lie on the tie lines between points (x, y) and V_2O_5 or $CuMoO_4$, respectively, which strongly supports the reliability of this analysis.

On the basis of the above findings a series of the xy-type solid solutions of composition listed in Table II was prepared and studied, as described in further paragraphs of the paper.

(ii) DTA

DTA of pure CuV_2O_6 agreed well with the earlier literature data (*3*, *17*). Endothermal peaks corresponding to the phase transformation (very weak effect) and incongruent melting were observed at 628 and 642°C, respectively; a liquidus line was reached at 740°C. As concerns the solid solutions $Cu^{2+}_{1-x-y}Cu^{1+}_{y}\phi_x V_{2-2x-y}Mo_{2x+y}O_6$, the effect of phase transformation has not been observed despite undoubtful evidence of this phenomenon with the high-temperature X-ray method (cf. Table III and the last paragraph of the paper). At temperatures 550–740°C the solid solutions show three or four endothermal effects. Since the determination of the phase diagram of this quaternary system would be a very ambitious undertaking, we restricted our studies to preliminary characterization of the solid solution thermal stability. The peaks appearing at the lowest temperature, listed in Table II as T_d, are thus assumed to correspond to the decomposition of solid solutions. The X-ray phase analysis of Mo-rich solid solutions annealed at 600°C, i.e., above T_d, reveals the presence of an admixture of a nonidentified compound.

(iii) Magnetic Susceptibility

The results of magnetic susceptibility measurements for pure CuV_2O_6 and ($x = 0.15$, $y = 0.25$) solid solution are shown in Fig. 3. The determined values of magnetic moment of Cu^{2+} ions amounting to 1.95 and 2.04 μ_B, respectively, are practically the same and characteristic of the bivalent copper (*16–18*). The Weiss constant is −40 K for both samples. The magnetic susceptibil-

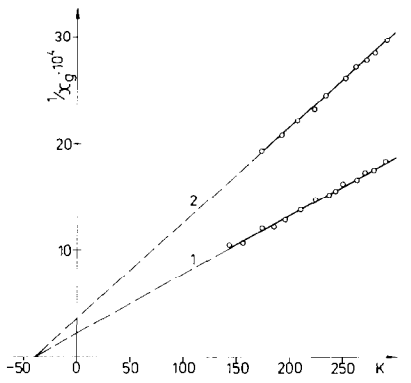

FIG. 3. Magnetic susceptibility of pure CuV_2O_6 (1) and ($x = 0.15$, $y = 0.25$) solid solution (2) as functions of temperature.

ity of 5.46×10^{-6}, as measured at 20°C for CuV_2O_6, is reduced by a factor 0.61 to $3.36 \cdot 10^{-6}$ for the solid solution studied; i.e., it is exactly proportional to the content of paramagnetic Cu^{2+} ions. As is seen from Fig. 3, this conclusion is valid for the whole temperature range studied. The results settle the questions of valence isomerism of the solid solution. They favor a valence structure $Cu^{2+}_{1-x-y}Cu^{1+}_{y}\phi_x V^{5+}_{2-2x-y}Mo^{6+}_{2x+y}O_6$ and rule out a description of the solid solution as $Cu^{2+}_{1-x}\phi_x V^{5+}_{2-2x-2y}V^{4+}_{y}Mo^{6+}_{2x+y}O_6$. In the latter formula the content of paramagnetic ions is much higher than in the former ($yCu^{2+} + yV^{4+}$). Thus the estimated χ_g should be greater than $6 \cdot 10^{-6}$, i.e., about twice as large as the experimental value ($3.36 \cdot 10^{-6}$). On the other hand, the second formula leads to the average Cu^{2+}–V^{4+} magnetic moment of 1.51 μ_B. This value is decidedly too small, the more so that μ_{eff} of V^{4+} ions surpass usually 2 μ_B due to the large orbital contribution (*18*).

(*iv*) X-*Ray Studies*

Table II lists the cell parameters and the triclinic–monoclinic phase transition temperatures, as determined with a high-temperature camera, for eight samples of the solid solution, ranging from a pure host compound CuV_2O_6 to a highly substituted structures. Multiple-regression analysis was used to establish correlations between the chemical composition (x, y) and variables listed in Table III, expressed as

$$z = a_0 + a_1x + a_2y.$$

Table III lists the regression coefficients, the maximum residual $(z - z_{obs})_{max}$ and the correlation index R^2. $(a_1/a) \cdot 100\%$ and

TABLE II

CELL DIMENSIONS AND TRANSITION TEMPERATURES FOR EIGHT SAMPLES OF $Cu^{2+}_{1-x-y}Cu^{1+}_{y}\phi_x V_{2-2x-y}Mo_{2x+y}O_6$ SOLID SOLUTION

Composition											
x	y	a (Å)	b (Å)	c (Å)	α (deg.)	β (deg.)	γ (deg.)	$c \sin\beta$ (Å)	V (Å^3)	T_t (°C)	T_d[a] (°C)
0	0	9.162(5)	3.553(2)	6.477(3)	92.31(1)	110.28(4)	91.82(5)	6.075	197.40	625	642
0.01	0.10	9.203(3)	3.573(1)	6.472(1)	92.07(2)	110.86(2)	91.49(3)	6.048	198.57	440	609
0.025	0.13	9.209(5)	3.584(1)	6.462(1)	91.89(2)	111.01(2)	91.32(4)	6.032	198.84	370	617
0.05	0.17	9.240(6)	3.592(1)	6.457(2)	91.68(2)	111.13(4)	91.14(3)	6.023	199.70	300	609
0.10	0.19	9.248(6)	3.606(2)	6.442(3)	91.44(5)	111.21(4)	91.11(7)	6.006	200.14	245	611
0.15	0.20	9.279(3)	3.618(1)	6.447(2)	91.25(3)	111.25(2)	90.69(4)	6.009	201.61	180	578
0.15	0.25	9.286(3)	3.625(1)	6.447(2)	91.01(2)	111.29(1)	90.76(3)	6.009	202.15	90	570
0.20	0.20	9.306(3)	3.631(1)	6.451(2)	90.91(2)	111.19(1)	90.70(2)	6.015	203.17	115	570
max (%)[b]		1.6	2.2	0.5	1.5	0.9	1.2	1.1	2.9	86	

[a] Temperature of "decomposition" as determined with DTA.

[b] For example, max c = [(6.477 − 6.442)/6.477] · 100%.

TABLE III

RESULTS OF REGRESSION ANALYSIS

Variable	Regression coefficients a_0	a_1	a_2	$(z - z_{obs})_{max}$	R^2	$\frac{a_1}{a_0} \cdot 100\%$	$\frac{a_2}{a_0} \cdot 100\%$
a	9.167	0.400	0.261	0.009	0.982	4.36	2.84
b	3.554	0.211	0.163	0.003	0.996	5.94	4.59
c	6.479	−0.033	−0.122	0.010	0.845	−0.51	−1.88
α	92.33	−4.560	−2.359	0.08	0.994	−4.94	−2.56
β	110.35	−0.820	4.806	0.14	0.955	−0.74	4.35
γ	91.79	−2.789	−2.704	0.14	0.963	−3.04	−2.94
$c \sin \beta$	6.073	0	−0.298	0.011	0.932	0	−4.90
V	197.54	21.197	5.431	0.55	0.979	10.73	2.75
T_t	617	−809	−1630	18	0.995	−131	−264

$(a_2/a) \cdot 100\%$ values are also included, as they reflect more clearly the relative changes in variables.

A simple inspection of Table II shows that two types of structural effects may be noticed along the studied series of solid solutions: (1) systematic evolution of the triclinic unit cell to the monoclinic one characteristic of brannerite-type compounds, and (2) expansion of the unit cell.

The first effect may be related to the decrease of concentration of Jahn–Teller Cu^{2+} ions which, as explained in the Introduction, are responsible for the triclinic distortion of the brannerite-type lattice. The second effect seems to be a result of introduction of ions differing in size as compared to those of the host structure. Ionic radii for Cu^{2+}, V^{5+}, and Mo^{6+} in octahedral environment, derived by Shannon and Prewitt (*19*) are 0.73, 0.54, and 0.60 Å, respectively. The ionic radius of 6-coordinated Cu^{1+} found by Rea and Kostiner (*20*) from the interatomic distance Cu–O in the $Cu^{1+}V^{5+}O_5$ structure is 0.76 Å. Both Cu^{1+} and Mo^{6+} are thus larger than Cu^{2+} and V^{5+}, respectively, although the difference between Mo^{6+} and V^{5+} is more significant than that between copper ions in the different valence states. Also, vacancies behave like ions of larger size because of an outward displacement of the neighboring oxygen ions.

It must be borne in mind that increases of x and y parameters in $Cu^{2+}_{1-x-y}Cu^{1+}_{y}\phi_x V_{2-2x-y}Mo_{2x+y}O_6$ reflect two different ways of the structure response to excess positive charge produced by substitution of Mo^{6+} for V^{5+}. These two ways are depicted in Fig. 4. It may be expected that both mechanisms should equally reduce the Jahn–Teller distortion, which depends primarily on the Cu^{2+} ion concentration. Path I (increase of x) should, however, bring about a more pronounced expansion component in relation to the electronic one since a removal of one Cu^{2+} ion gives rise to the incorporation of two large Mo^{6+} and one large void. This is in contrast to mechanism II, where one Cu^{2+} ion is replaced by a slightly different Cu^{1+} ion, which is accompanied by incorporation of only one Mo^{6+}. The values of regression coefficients given in Table III confirm our expectations. The unit cell volume depends primarily on x. The regression coefficient for x has a magnitude about four times that for y. The enlargement of the unit cell is primarily a consequence of the expansion in the a and b cell dimensions, since c, $\sin \alpha$, $\sin \beta$, and $\sin \gamma$ change insignificantly. Both a and b

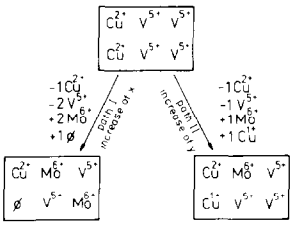

FIG. 4. Two paths of the excess-charge compensation produced by substitution of Mo^{6+} for V^{5+} in CuV_2O_6.

are affected more by x than by y. The most pronounced dilatation of the structure occurs in the direction of the b axis, which corresponds to an elongation of the chains of corner-shared VO_6 and edge-shared CuO_6 octahedra. This is in fair agreement with similar data for the $Mn_{1-x}\phi_xV_{2-2x}Mo_{2x}O_6$ solid solution which is stoichiometrically equivalent to the substitution scheme I, and in which changes in the cell dimensions are mainly governed by ionic size effects.

The changes in α, β, γ seem to result from the declining Jahn–Teller distortion in the course of substitution. Angles α and β approach 90° across the series with comparable x- and y-dependent contribution. The β angle increases along the series becoming closer to β values typical of brannerite-type structures (111–112°). In the $Mn_{1-x}\phi_xV_{2-2x}Mo_{2x}O_6$ system the dilatation of the lattice on increasing x is accompanied by β-angle diminution. In our case, x-dependent contribution is also negative, although very small, and β increases due to the large positive y-dependent contribution.

The final point to present is the influence of x and y on the $\alpha \rightleftarrows \beta$ transition temperature. Starting from 625°C for pure CuV_2O_6, T_t decreases abruptly with an increase in x and y. The regression coefficient for y has a magnitude about twice that for x. It is not surprising that T_t is correlated with both x and y as both substitution components lead to the decrease of the concentration of Jahn–Teller Cu^{2+} ions in the structure, which facilitates the transition to the dynamically distorted structure with higher symmetry, favored at higher temperatures. The more pronounced contribution of y than x to the transition temperature decrease results obviously from different substitution schemes which accompany a removal of Cu^{2+} ions.

References

1. C. CALVO AND D. MANOLESCU, *Acta Crystallogr. Sect. B* **29**, 1743 (1973).
2. R. KOZŁOWSKI, J. ZIÓŁKOWSKI, K. MOCAŁA, AND J. HABER, *J. Solid State Chem.* **35**, 1 (1980), and references cited therein.
3. D. MERCURIO, J. GALY, AND B. FRIT, *C.R. Acad. Sci. Paris Ser. C* **282**, 27 (1976).
4. D. REINEN, *J. Solid State Chem.* **27**, 71 (1979).
5. J. ZIÓŁKOWSKI, R. KOZŁOWSKI, K. MOCAŁA, AND J. HABER, *J. Solid State Chem.* **36**, 297 (1980).
6. B. DARRIET AND J. GALY, *Bull. Soc. Fr. Minéral. Crystallogr.* **91**, 325 (1968).
7. J. GALY, J. DARRIET AND B. DARRIET, *C.R. Acad. Sci. Paris Ser. C* **264**, 1477 (1967).
8. Joint Committee on Powder Diffraction Standards 1973, 5-661, 9-387, 5-508.
9. S. C. ABRAHAMS, J. L. BERNSTEIN, AND P. B. JAMIESON, *J. Chem. Phys.* **48**, 2619 (1968).
10. K. NASSAU AND S. C. ABRAHAMS, *J. Cryst. Growth* **2**, 136 (1968).
11. D. MERCURIO-LAVAUD AND B. FRIT, *Acta Crystallogr. Sect. B* **29**, 2737 (1973).
12. B. RAVEAU, *Rev. Chim. Minér.* **4**, 729 (1967).
13. L. DZIEMBAJ AND J. ZIÓŁKOWSKI, *Bull. Acad. Polon. Sci. Ser. Sci. Chim.* **20**, 725 (1972).
14. T. MACHEJ AND J. ZIÓŁKOWSKI, *J. Solid State Chem.* **31**, 135 (1980).
15. N. F. CURTIS, *J. Chem. Soc.*, 3147 (1961).
16. P. W. SELWOOD, "Magnetochemistry," Interscience, New York/London (1956).
17. C. BRISI AND A. MOLINARI, *Ann. Chim.* **48**, 263 (1958).
18. M. M. SCHIEBER, "Experimental Magnetochemistry," North-Holland, Amsterdam (1967).
19. R. D. SHANNON AND C. T. PREWITT, *Acta Crystallogr. Sect. B* **25**, 925 (1969).
20. J. R. REA AND E. KOSTINER, *J. Solid State Chem.* **7**, 163 (1973).